

Calcium oscillation on homogeneous and heterogeneous networks of ryanodine receptor

Zhong-Xue Gao,^{*} Tian-Tian Li,^{*} Han-Yu Jiang,[†] and Jun He[‡]
School of Physics and Technology, Nanjing Normal University, Nanjing 210097, China

 (Received 26 July 2022; revised 28 November 2022; accepted 20 January 2023; published 6 February 2023)

Calcium oscillation is an important calcium homeostasis, imbalance of which is the key mechanism of initiation and progression of many major diseases. The formation and maintenance of calcium homeostasis are closely related to the spatial distribution of calcium channels on endoplasmic reticulum, whose complex structure was unveiled by recent observations with superresolution imaging techniques. In the current paper, a theoretical framework is established by abstracting the spatial distribution of the calcium channels as a nonlinear biological complex network with calcium channels as nodes and Ca^{2+} as edges. A dynamical model for a ryanodine receptor (RyR) is adopted to investigate the effect of spatial distribution on calcium oscillation. The mean-field model can be well reproduced from the complete graph and dense Erdős-Rényi network. The synchronization of RyRs is found important to generate a global calcium oscillation. Below a critical density of the Erdős-Rényi or Barabási-Albert network, the amplitude and interspike interval decrease rapidly with the end of disappearance of oscillation due to the desynchronization. The clique graph with a cluster structure cannot produce a global oscillation due to the failure of synchronization between clusters. A more realistic geometric network is constructed in a two-dimensional plane based on the experimental information about the RyR arrangement of clusters and the frequency distribution of cluster sizes. Different from the clique graph, the global oscillation can be generated with reasonable parameters on the geometric network. The simulation also suggests that existence of small clusters and rogue RyRs plays an important role in the maintenance of global calcium oscillation through keeping synchronization between large clusters. Such results support the heterogeneous distribution of RyRs with different-size clusters, which is helpful to understand recent observations with superresolution nanoscale imaging techniques. The current theoretical framework can also be extended to investigate other phenomena in calcium signal transduction.

DOI: [10.1103/PhysRevE.107.024402](https://doi.org/10.1103/PhysRevE.107.024402)

I. INTRODUCTION

Calcium homeostasis is the key mechanism to maintain life-sustaining activities. Its imbalance is responsible for the initiation of many major diseases, such as neurodegenerative and cardiovascular diseases [1–3]. As an important calcium homeostasis, calcium oscillation is a ubiquitous signal in all cells, and provides efficient means to transmit intracellular biological information through its amplitude and frequency, therefore attracting much attention [4–7]. Many models have been proposed to study the calcium signaling transduction and the formation of calcium homeostasis [8–13]. In the existing models, the calcium channels, such as ryanodine receptors (RyRs) and inositol 1,4,5-trisphosphate receptors (IP_3R), play an important role in the regulation of intracellular calcium concentration. After inclusion of other mechanisms, such as calcium bump, calcium leak, and mitochondrion, the phenomena of calcium homeostasis, including calcium oscillation, were reproduced from many proposed models to explain experimental observations [8,9,14–16].

Most existing models were constructed under the mean-field ansatz [8–11]. In such models, the calcium concentrations near all calcium channels are set to be the same value, and all channels behave in the same manner. It requires homogeneous distribution of the channels on the endoplasmic reticulum, which obviously conflicts with the experimental observations that the calcium channels exhibit a cluster structure composed of several to tens of channels [17–20]. Such a heterogeneous cluster structure makes the intracellular calcium signaling exhibit obvious hierarchy. Many models have been proposed to simulate such a structure [12,13,21–23]. For example, using deterministic-stochastic simulations, Rüdiger *et al.* studied local calcium signaling in a cluster with compact distribution of the channels in a rectangle, and well described calcium puffs in neuronal cells [12].

These studies about the cluster structure deepen our understanding of the hierarchy of calcium signaling. However, recent superresolution observations suggest that the clusters have a more complex internal structure. In many studies, the cluster is assumed to be packed compactly [12,21–24], forming a tight lattice as suggested by early experimental observations [17,18], which means that the mean-field ansatz is still suitable to study the local dynamics in a cluster, at most with some small modifications. However, recent superresolution nanoscale imaging shows that the accurate characteristics of calcium-channel arrangement in a cluster are not trivial

^{*}These authors have contributed equally to this work.

[†]Corresponding author: jianghy@njnu.edu.cn

[‡]junhe@njnu.edu.cn

and should be considered seriously [20,25]. The cluster is not compact, has irregular shape, and different sizes with randomness. In Refs. [26,27], activation of RyRs was found to be sensitive to the arrangement of RyRs in a cluster. Their study suggests that a regular compact picture of cluster and mean-field approximation are not suitable for simulation of RyR arrangement observed experimentally. The RyR arrangement is also very important in the regulation of calcium-induced calcium release. The simulations in previous research give contradictory results [28,29]. Hence, the explicit arrangement of calcium channels in a cluster needs more investigation.

The cluster size (the number of calcium channels in a cluster) is another important index of the cluster, and was found to have a close relationship to the diseases, such as Niemann-Pick type C1 [25]. In Ref. [30], the local calcium release from clusters with a few IP₃R channels was studied, and nonlinearity was found for the interpuff interval and the first puff latency against the inverse cluster size. The effect of cluster sizes of both RyRs and IP₃R was also studied in the literature [21–23,31,32]. In recent years, more experiments were performed to study the frequency distribution of cluster sizes [18,20,25,33]. Besides clusters with large sizes, which have been observed in early experiments, many rogue RyRs, as well as many small clusters, were also found in recent observations. It has significance to study their roles in calcium-signaling transduction. A recent study suggests that rogue RyRs greatly increase the initiation of Ca²⁺ sparks, further contributing to the formation and propagation of Ca²⁺ waves [34]. More interestingly, recent superresolution imaging shows a phenomenon that the frequency distribution is exponential to the cluster size, that is, it obeys the power law [18,20]. It means that the clusters with one to several RyRs constitute the majority of all clusters.

In the existing works, many studies focused on the dynamics in a cluster. However, the effect of the spatial distribution of calcium channels, such as the frequency distribution of cluster sizes, are beyond a cluster. With the development of superresolution imaging techniques, more information about calcium channel distribution will be achieved in the future. It is urgent to carry out systematic and appropriate simulation research beyond the existing models to investigate irregular and random distributions of channels, which is scarce in the literature. If we go beyond the local cluster and mean-field ansatz, a unified description of channel distribution at different scales should be constructed. In fact, the effect of channel distribution on the calcium-signaling transduction can be reflected by Ca²⁺ connections between calcium channels. If we know the effect of other channels on the calcium concentration near the channel considered, the channel distribution can be described without loss of spatial information. The Ca²⁺ connections between calcium channels can be abstracted as the edges of a network with the channels as nodes. The connection strength corresponds to a weighted edge or the probability of connection by an unweighted edge.

In the literature, there exist some attempts to study the calcium signal transduction on the network of calcium channels. In Refs. [22,23], an adjacency matrix was introduced to model calcium release in the heart. In fact, it equals a network, but only the connections between adjacent RyRs were considered. Such treatment can be also found in Refs. [26,27]

with more RyRs involved. However, only simulation for a single cluster was performed to study the calcium spark (blip). In Ref. [35], with a simple two-state model of the receptor, a bistable regime can emerge from the network dynamics with several classical network architectures. By introducing the Keizer-Levine model [9], where a simplified mechanism mimicking adaptation has been developed to reproduce experimental data from cardiac cells under a mean-field ansatz, in our previous work the Ca²⁺ induced Ca²⁺ release was studied to explore the behavior of signaling networks with multistates in which nodes are regulated by reaction rates nonlinearly [36].

The studies suggest that different architectures of the network will affect the bistable regime [35,36]. However, the calcium oscillation was not reproduced in these models because only the state transition of calcium channel was considered. To reproduce the calcium oscillation, more mechanisms, such as store leak and calcium pump, should be included to form an open-cell model [9]. Influx and efflux of Ca²⁺ from an external medium should be also considered to construct a more realistic model. Under the mean-field ansatz, the Keizer-Levine model successfully generates the calcium oscillation with these ingredients [9]. In this paper, we will establish a theoretical frame to describe channel distribution by a nonlinear network. The Keizer-Levine model will be extended to a network model to include the effect of spatial distribution (Sec. II). The network with full connections, that is, complete graph, will be introduced to check the model.

With the established theoretical frame, three classical networks which reflect different sides of spatial distribution of calcium channels will be introduced to study their effect on calcium oscillation in Sec. III. The Erdős-Rényi network is introduced to check the equivalence of a homogeneous network with the mean-field approximation. The heterogeneous Barabási-Albert network is known for its scale-free characteristic [37]. It is introduced to reflect the power law of the frequency distribution of cluster sizes if a cluster is taken as a node. Another heterogeneous network, a clique graph with nodes in a clique being fully connected, is also introduced to simulate the compact clusters which have the same size, and connect to other clusters weakly due to the large intercluster distance. In Sec. IV, a more realistic model will be constructed in a two-dimensional plane based on the experimental information about the internal RyR arrangement of the cluster and the frequency distribution of cluster sizes. The connections will be determined by calcium concentration gradient. With such a geometric network, the role of clusters with small sizes will be investigated. The discussion of the results and a summary can be found in Sec. V.

II. MECHANISM OF CALCIUM REGULATION

A. General form

First, we present a general form of a calcium regulation mechanism on a network. The transition of a calcium channel, RyR or IP₃R, between its different states is a kernel mechanism to reproduce the calcium oscillation. The calcium channel has two basic states, open and closed. The Ca²⁺ is released from a channel in the open state. However, in a

realistic model, there are often more states required. Here, we assume that there exist M states for a channel. As in Ref. [36], we express the state as a vector $V = [0, \dots, 1, \dots, 0]$ with one of its M elements being 1 and others being 0. $V_m = 1$ means that the channel is in state m . For a system with N channels, the total state of the system can be described by a matrix $R_{im} = V_m^i$, with $i = 1, 2, \dots, N$ and $m = 1, 2, \dots, M$.

The master equation for the state transition of calcium channel i can be generally written as

$$\frac{d\mathcal{P}_m^i(R_{im}, t)}{dt} = \sum_n T_{mn}^i([Ca^{2+}]_i) \mathcal{P}_n^i(R_{im}, t), \quad (1)$$

where $\mathcal{P}_m^i(R_{im}, t)$ is the probability of system in a state R_{im} at a time t . The transition rate for node i between states m and n is described by the element in m row and n column of a transition rate matrix $T^i([Ca^{2+}]_i)$, which is dependent on the calcium concentration $[Ca^{2+}]_i$ at channel i . In different models, the transition rate matrix $T^i([Ca^{2+}]_i)$ can be different.

To determine the transition probability of a channel, the variation of calcium concentration $[Ca^{2+}]_i$ near this channel is required. The flux from other open channels should be considered. It will take some time before the calcium ions released from an open channel diffuse to another channel. In the literature, the connection between an open channel and the channel considered was often treated by the diffusion equation. However, the calcium signaling propagates mainly with the calcium-induced calcium-release mechanism, that is, the Ca^{2+} propagation between two neighbor channels is more important. Besides, the diffusing Ca^{2+} may attach into the buffers, such as calmodulin, and no longer affect the calcium channels until deattaching. The results in our previous work [38,39] suggest that the Ca^{2+} released from an open channel will disperse rapidly with increasing distance. Hence, the effect of calcium ions released from an open channel is constrained in a small region. As shown in Refs. [18,20], the cluster diameter and distance of the nearest-neighbor clusters have the largest distribution at values of 100 nm and 200 nm, respectively, and the mean distance between RyRs in a cluster is about 40 nm. With the diffusion constant $D_{Ca} = 200 \mu m^2/s$, we can estimate the diffusion time as $t = r^2/2D_{Ca}$. The above distances correspond to times 0.025, 0.1, and 0.00004 ms, respectively. The diffusion delay between the channels and clusters should be very small compared with the mean RyR open time, about 2.2 ms [40]. It was also discussed in Refs. [27,41,42] that the activation of RYRs after an RYR opening proceeds much slower than the buildup of the calcium gradient. Hence, the diffusion delay between the RyRs around the open RyR can be safely neglected, especially for the calcium oscillation considered here. In the current paper, the variation of calcium concentration $[Ca^{2+}]_i$ near a channel is determined by the calcium gradient induced from open channels, and the time delay is neglected.

After neglecting the delay, the Ca^{2+} connections between channels can be further abstracted as edges of a complex network with calcium channels as nodes. There exist two means to describe the Ca^{2+} connections, the weighted and unweighted edges. The weight of a weighted edge can be determined by the calcium concentration directly. In the current paper, to introduce classical networks, the unweighted

networks will be adopted in calculation. In such networks, if a channel pair has possibility p to be connected by Ca^{2+} , the corresponding element of adjacency matrix A_{ij} has a possibility p to be 1. For the channel pair with no Ca^{2+} connection, the element is set as 0. The treatment will be explained more explicitly in Sec. IV. Obviously, such a network is an undirected network. Hence, for a channel i , the Ca^{2+} flux received from other open channels can be written as

$$J_i^R([Ca^{2+}]_j) = \sum_{jm} \gamma_j([Ca^{2+}]_j) A_{ij} R_{jm}. \quad (2)$$

It is determined by release rate $\gamma_j([Ca^{2+}]_j)$ of all open channels j which have connections to channel i , including i itself if it is open. Such flux leads to the increase of calcium concentration near channel i .

In the realistic model, more mechanisms, such as store leak, calcium pump, and exchange with the external medium, should be included to form an open-cell model where the oscillation can occur. The total variation of the calcium concentration near channel i can be described as

$$\frac{d[Ca^{2+}]_i}{dt} = J_i^R([Ca^{2+}]_j) + J_i'([Ca^{2+}]_i). \quad (3)$$

The Ca^{2+} flux from these mechanisms is denoted as $J_i'([Ca^{2+}]_i)$. In a realistic model, explicit positions about calcium pumps should be introduced, for example, the distance between the calcium pump and calcium channel. In the current paper, we focus on the mechanism of the state transition of calcium channels on network. $J_i'([Ca^{2+}]_i)$ is assumed to be only dependent on the calcium concentration near channel $[Ca^{2+}]_i$ for simplification.

B. Mean-field ansatz

To understand the basic features of network dynamics, we first provide the approximate results under a simple spatially homogeneous mean-field ansatz. Under this ansatz, all nodes, i.e., the calcium channels, are assumed to evolve with time in the same manner. If starting from a spatially homogeneous initial calcium concentration, the equation for the variation of the calcium concentration in Eq. (3) should be the same for every node, that is, independent on i and j . Therefore, the calcium concentration $[Ca^{2+}]_i$ should evolve homogeneously. The release rate $\gamma_j([Ca^{2+}]_j)$ is then deduced to $\gamma([Ca^{2+}])$. The Ca^{2+} flux received from other open channels in Eq. (2) can be rewritten as

$$J_i^R = \gamma([Ca^{2+}]) \sum_{jm} A_{ij} R_{jm}. \quad (4)$$

The state matrix R_{jm} is deduced into R_{1m} for all nodes, that is, all nodes have the same state m at a time point (here, we take state of node 1 as representative value). We reach

$$\sum_{jm} A_{ij} R_{jm} = \sum_j A_{ij} \sum_m R_{1m} = \langle k \rangle \sum_{m=0} p_m. \quad (5)$$

Here we apply average degree $\langle k \rangle = \frac{1}{N} \sum_{ij} A_{ij} = \sum_j A_{ij}$ and the fraction of channels in state m is defined as $p_m = \frac{1}{N} \sum_i R_{im} = R_{1m}$ due to the spatial homogeneity under the mean-field ansatz. Since only the open channel can release Ca^{2+} , only open states with $m = O$ are kept. Equation (3) for

TABLE I. Transition rate matrix $T([\text{Ca}^{2+}])$ with parameters $k_a^+ = 1500 \mu\text{M}^{-4}\text{s}^{-1}$, $k_a^- = 28.8 \text{ s}^{-1}$, $k_b^+ = 1500 \mu\text{M}^{-3}\text{s}^{-1}$, $k_b^- = 385.9 \text{ s}^{-1}$, $k_c^+ = 1.75 \text{ s}^{-1}$, and $k_c^- = 0.1 \text{ s}^{-1}$ [9].

State	C_1	O_1	C_2	O_2
C_1	$-k_a^+[\text{Ca}^{2+}]^4$	k_a^-		
O_1	$k_a^+[\text{Ca}^{2+}]^4$	$-k_a^- - k_b^+[\text{Ca}^{2+}]^3 - k_c^+$	k_c^-	k_b^-
C_2		k_c^+	$-k_c^-$	
O_2		$k_b^+[\text{Ca}^{2+}]^3$		$-k_b^-$

the variation of calcium concentration under the mean-field ansatz can be written as

$$\frac{d[\text{Ca}^{2+}]}{dt} = \gamma([\text{Ca}^{2+}])\langle k \rangle \sum_{m=O} p_m + J'([\text{Ca}^{2+}]). \quad (6)$$

The master equation for the state transition of the calcium channel in Eq. (1) is deduced to an equation of the fractions of channels in different states as

$$\frac{dp_m(t)}{dt} = \sum_n T_{mn}([\text{Ca}^{2+}]) p_n(t). \quad (7)$$

To determine the explicit form of the flux $J^R([\text{Ca}^{2+}])$, $J'([\text{Ca}^{2+}])$, and transition rate matrix $T([\text{Ca}^{2+}])$, we compare the general form of the mechanism under the mean-field ansatz in Eqs. (6) and (7) with the Keizer-Levine model, which is also under the mean-field ansatz [9]. In the Keizer-Levine model, four states of the RyR are introduced as C_1 , O_1 , C_2 , and O_2 to describe the experimental phenomena. The closed state C_1 is dominant at a low concentration $[\text{Ca}^{2+}]$, for example, $0.1 \mu\text{M}$. If the $[\text{Ca}^{2+}]$ increases, the RyR is activated from the closed state C_1 to an open state O_1 at a rate of $k_a^+[\text{Ca}^{2+}]^4$ and deactivates back to C_1 state at a rate of k_a^- . As suggested in Ref. [9], to keep the plateau, the open state O_1 also may be activated to the second open state O_2 at a rate of $k_b^+[\text{Ca}^{2+}]^3$ and back to the first open state O_1 at a rate of k_b^- . It is also important to obtain the bistable regime [36]. To describe the adaption phenomenon, the transition between the first open state O_1 and the second closed state C_2 is also added. The transition rates between these states are described by the transition rate matrix $T([\text{Ca}^{2+}])$ as listed in Table I. With the experimental data of Györke and Fill [43], the RyR kinetic constants $K_{(a,b,c)}^\pm$ have been determined in Ref. [9], which are also given in Table I. By comparing the Ca^{2+} flux from the RyRs in the Keizer-Levine model [9] and that under the mean-field ansatz in Eq. (6), the transition rate of channels can be determined as

$$\gamma([\text{Ca}^{2+}]) = f \nu_1'([\text{Ca}_s^{2+}] - [\text{Ca}^{2+}]), \quad (8)$$

where a factor $f = 0.01$ is introduced as the fraction of Ca^{2+} that is free in the cytoplasm [44]. The ν_1' is the release rate constant for the RyRs. We would like to emphasize that the definitions of release rate under the mean-field ansatz and for a single channel should be different. The ν' is realistic release rate constant which reflects the ability of a channel receptor. The ν_1 adopted under the mean-field ansatz is, in fact, an effective quantity, and dependent on the average degree $\langle k \rangle$. In the current work, we relate the release rate for a channel to

that under the mean-field ansatz as $\nu_1' = \nu_1/\langle k \rangle$. The ν_1 was determined as 40 s^{-1} based on Friel's analysis of the bullfrog sympathetic neuron [45]. With such relation, the mean-field approximation of a network will be deduced to the Keizer-Levine model.

As in Eq. (8), the release of calcium from the RyRs is assumed to be proportional to the concentration gap between cytoplasm and store, i.e., $[\text{Ca}^{2+}]$ and $[\text{Ca}_s^{2+}]$. The calcium concentration of store is assumed as $[\text{Ca}_s^{2+}] = (C_0 - [\text{Ca}^{2+}])/c_1$. The factor c_1 is sometimes referred to as the ratio of effective volume of the store to the cytoplasm, and is determined as 0.15 based on the experimental data in Ref. [46]. The C_0 is the total free- Ca^{2+} concentration in the cell. If the cell is open to external medium, it should not be fixed, but vary with influx and efflux from the plasma membrane calcium (PMCA) pump according to the equation [9]

$$\frac{dC_0}{dt} = f \left(j_{\text{in}} - \nu_{\text{out}} \frac{[\text{Ca}^{2+}]^2}{[\text{Ca}^{2+}]^2 + K_{\text{out}}^2} \right), \quad (9)$$

with j_{in} being the influx rate, which has a value $j_{\text{in}} = 1 \mu\text{Ms}^{-1}$ obtained from a current of 0.1 pA in a cell with a volume of $1000 \mu\text{m}^3$. ν_{out} and K_{out} are the maximal rate and dissociation constant of the PMCA pump, and chosen as $9.0 \mu\text{Ms}^{-1}$ and $0.6 \mu\text{Ms}$, respectively [9,47,48].

Besides the exchange of Ca^{2+} with external medium, the Ca^{2+} exchange with the calcium store should be included. Hence, the flux $J'[\text{Ca}^{2+}]$ can be described as [9]

$$J'[\text{Ca}^{2+}] = f \left(\nu_2([\text{Ca}_s^{2+}] - [\text{Ca}^{2+}]) - \nu_3 \frac{[\text{Ca}^{2+}]^2}{[\text{Ca}^{2+}]^2 + K_3^2} + j_{\text{in}} - \nu_{\text{out}} \frac{[\text{Ca}^{2+}]^2}{[\text{Ca}^{2+}]^2 + K_{\text{out}}^2} \right). \quad (10)$$

The first and second terms are for the calcium leak from calcium store, and returning Ca^{2+} to the calcium store through the sarcoplasmic endoplasmic reticular calcium ATPase (SERCA) pump, respectively. The third and fourth terms are the influx and efflux of Ca^{2+} exchange with the external medium, respectively, as in Eq. (9). Here the dissociation constant of SERCA pump $K_3 = 0.3 \mu\text{M}$ [49]. ν_2 and ν_3 are the rate constants for store leak and the SERCA pump, and chosen as $0.1 \mu\text{Ms}^{-1}$ and $120 \mu\text{Ms}^{-1}$, respectively [9].

The calcium oscillation produced with a set of the parameters under the mean-field ansatz is presented in Fig. 1. Different from the original Keizer-Levine model, in our calculation, Eqs. (6) and (7) are adopted directly without separation between fast and slow timescales. As discussed above, in Eq. (8), the release rate of RyRs under the mean-field ansatz can be related to the average degree of the network. Here, we present the results with different release rates under the mean-field ansatz. As shown in Fig. 1, the calcium oscillation can be reproduced with the ν_1 considered, and very close to the results with separation between fast and slow timescales [9]. One can find that larger release rates result in the calcium oscillation with a smaller interspike interval and smaller amplitude. With the increase of release rate ν_1 from 20 to 50 s^{-1} , relaxation time of the oscillation becomes small.

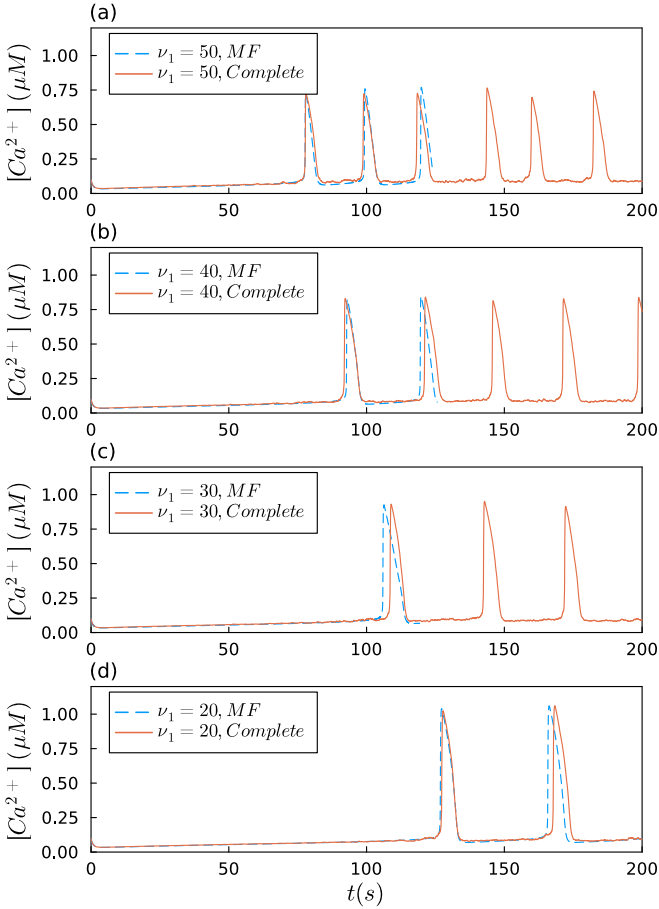


FIG. 1. Calcium oscillation in mean-field ansatz (MF) and on the complete graph network with different release rate constant of RyRs under mean field ansatz as $\nu_1 = 50, 40, 30,$ and 20 s^{-1} in (a)–(d), respectively.

C. Calcium oscillation on complete graph network

The complete graph with full connections between nodes is introduced here to check the network model. Obviously, such a network is homogeneous and only dependent on the number of nodes. Since the calcium concentration near a channel will increase with the total number of channels, the complete graph is only appropriate to describe a small system, such as a compact cluster, but cannot be applied to the channel distribution at a large scale. However, it can be well described by the mean-field approximation and used to check the network formalism adopted in the current paper. The results on this network should fit well with the mean-field approximation, with $\nu'_1 = \nu_1/(N-1)$ for large channel number N , which is chosen as 1000 in the current paper. Under the mean-field ansatz, the $[\text{Ca}^{2+}]_i$, $\gamma_j([\text{Ca}^{2+}]_j)$, and $J'_i([\text{Ca}^{2+}]_i)$ are the same for all channels. After the network is introduced, these quantities should be set differently for every channel. After inserting them into Eqs. (1)–(3), one can reach a formalism for the calcium signaling on a network.

In the current paper, we adopt the Julia language to perform simulations. The Gillespie algorithm is employed to deal with the transition of RyR states. There exist $n_r = 6$ types of transitions between different states of every channel as shown in

Table I. Hence, at a certain time point, total $n = N \sim n_r = 6000$ events may occur; the possibility for each event can be obtained with the transition rate and propensity as α_i with i from 1 to n . As usual with the Gillespie algorithm [50], two random numbers r_1 and r_2 are generated. One of them, r_2 , is used to judge which event will occur. If $\sum_{i=1}^{j-1} \alpha_i \leq r_2 \alpha \leq \sum_{i=1}^j \alpha_i$ with total possibility $\alpha = \sum_{i=1}^n \alpha_i$, the i th event occurs. Another r_1 is used to generate the time interval until the next event as $\Delta t = -\log r_1/\alpha$. The calcium concentration $[\text{Ca}^{2+}]_i$ and C_{0i} also have variations $\frac{d[\text{Ca}^{2+}]_i}{dt}|_t \Delta t$ and $\frac{dC_{0i}}{dt}|_t \Delta t$. With such an algorithm, the calcium concentration and the state of each RyR evolve with time t .

The results with the complete graph are also presented in Fig. 1. As shown in Eq. (8), to compare the results with these in the mean-field approximation, the release rate ν_1 is divided by the average degree $\langle k \rangle$. Under such definition, the model with complete graphs corresponds to the mean-field approximation with the same value of ν_1 . The global calcium concentration is defined as the average of all RyRs, $[\text{Ca}^{2+}] = \sum_{i=1}^N [\text{Ca}^{2+}]_i/N$. As expected, the result shows that simulation of global calcium concentration with complete graphs produces almost the same interspike time and amplitude as the mean-field approximation. The interspike time and amplitude with the mean-field approximation are identical for each period while little deviation can be found for the simulation with the network due to the uncertainties of the random numbers introduced in the Gillespie algorithm. Decrease of the interspike interval and amplitude can be found with the increase of the release rate ν_1 .

III. CALCIUM OSCILLATION ON CLASSICAL NETWORKS

The complete graph can be related to a compact cluster in which all channels are connected to each other. The above calculation suggests that such a structure can be well described by the mean-field approximation as in Ref. [26]. In the current paper, the spatial distribution of the calcium channels beyond the cluster is considered, which is very complex. The intracellular space is crowded with various obstructions and organelles [51]. The diffusing Ca^{2+} has to navigate between these complex intracellular structures. Most of the calcium channels distribute on the smooth endoplasmic reticulum with a complex three-dimensional network structure [33]. Even for the rough endoplasmic reticulum with a flat layer shape, its folding structure in the cytoplasm makes some parts of different sheets very close to each other [52]. Ca^{2+} can be communicated between distant regions of endoplasmic reticulum. Combined with the cluster structure, the connections between calcium channels should be very complex and suitable to be described as a complex network.

With the theoretical frame constructed in the above section, in this section, three classic networks will be introduced to study the effect of different network architectures on the calcium oscillation. In this section, the homogeneous Erdős-Rényi network, heterogeneous Barabási-Albert, and clique graph networks [53] will be considered to reflect the characteristics of spatial distribution of calcium channels. The procedure to study these networks is almost the same as the

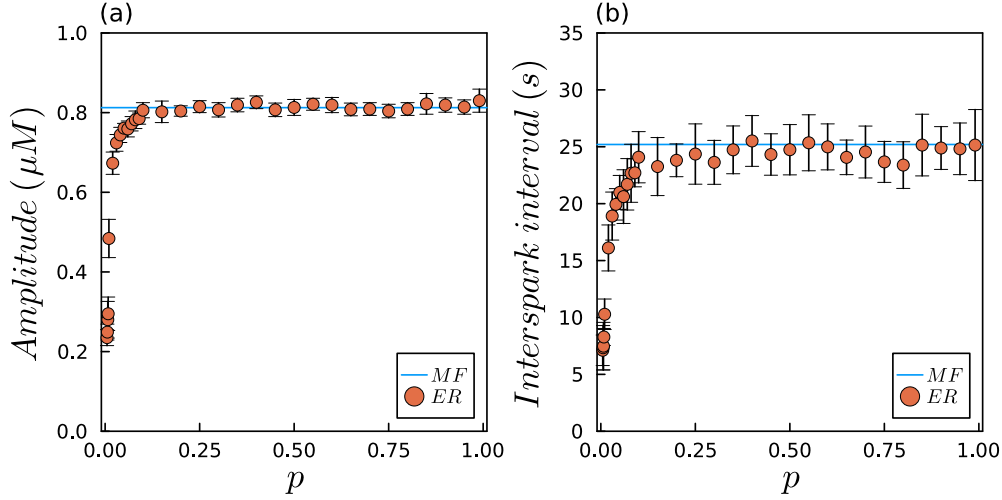


FIG. 2. Average amplitude and interspike interval of calcium oscillation on the Erdős-Rényi (ER) network with the variation of possibility p . The values in the mean-field approximation are given as horizontal lines. Other parameters are chosen as those in Fig. 1 with $\nu_1 = 40 \text{ s}^{-1}$ and $N = 1000$.

complete graph after the adjacency matrix A is replaced. In the following simulations, the networks and its adjacency matrix will be generated with the GRAPHS package of the JULIA Lagrangian. And the diagonal elements will be set 1 to include the effect the channel itself.

A. Erdős-Rényi network

The Erdős-Rényi network with N nodes, denoted as $G_{\text{ER}}(N, p)$, is generated by adding edges into the node pairs with a possibility p . It is homogeneous because every node in the network has equal status. The Erdős-Rényi network can describe the characteristic of channel distribution at large scale where the mechanism of calcium regulation can be successfully described in the mean-field approximation. Different from the complete graph, the Erdős-Rényi network is not completely connected and randomness is introduced. As a homogeneous network such as the complete graph, the behavior of evolution of calcium concentration should also be analogous to those in the mean-field approximation. In Fig. 2, an average amplitude of ten spikes and average interspike interval of ten periods with the variation of possibility p are presented with the standard deviations.

In Fig. 2, one can find that in a large range of possibility p larger than 0.1, the amplitude is about $0.8 \mu\text{M}$ and the interspike interval is about 25 s, which fit the mean-field approximation as expected. However, if the possibility p becomes very small, both amplitude and interspike intervals decrease rapidly and the oscillation disappears rapidly. In the current paper, we fix the release rate constant ν_1 in the mean-field approximation at 40 s^{-1} , and the rate for the network can be obtained as $\nu'_1 = \nu_1 / \langle k \rangle$. For the Erdős-Rényi network, the average degree $\langle k \rangle = p(N - 1)$, which means that the large possibility p leads to small release rate constant ν'_1 for calcium channels, which are nodes of the network. Hence, on a denser network, smaller ability of transporting calcium ions is required.

To provide a more explicit picture about the oscillation on the network, in Fig. 3, the evolution of calcium concentration $[\text{Ca}^{2+}]$ on the Erdős-Rényi network is presented. The calcium concentration $[\text{Ca}^{2+}]_i$ for every node, i.e., near every channel, is also illustrated.

Since the dense networks with large p values show similar behaviors as suggested in Fig. 2, only some selected small p values are considered. As expected, on the network $G_{\text{ER}}(1000, 0.1)$, the evolution of global calcium concentration with time t is similar to these in the mean-field approximation in Fig. 1(b), which can be digitalized as amplitude and interspike interval close to the values in mean-field approximation in Fig. 2. The evolution of calcium concentration with time for each channel exhibits almost the same behavior as shown in Fig. 3(b), which indicates the synchronization of the system, and results in a wonderful global oscillation.

Increase of sparsity will reduce the homogeneity of network. On the network $G_{\text{ER}}(1000, 0.01)$, the oscillation is still reproduced well with a smaller interspike interval and amplitude, which deviate from the mean-field approximation. Moreover, a few nodes do not behave in the same manner as the majority, which makes the fringes fluffy, as shown in Fig. 3(d). It reflects the appearance of desynchronization. With the decrease of the p value, the network becomes sparser, and the synchronization of nodes is broken down gradually. On the network $G_{\text{ER}}(1000, 0.005)$, more nodes are out of synchronization, which makes the oscillation of the global calcium concentration unobvious. On the network $G_{\text{ER}}(1000, 0.002)$, where some nodes are even not connected, the synchronization is almost broken down totally, and the global oscillation of calcium concentration disappears also, as shown in Fig. 3(h).

We make a simple check about the effect of node number of the system. The results are presented in Figs. 2(a), 2(c), 2(e), and 2(f) as dashed red lines. In these simulations, only 500 nodes are considered, which is a half of the node number in the above simulation. At the same time, the connection possibility p is doubled to keep the average degree unchanged.

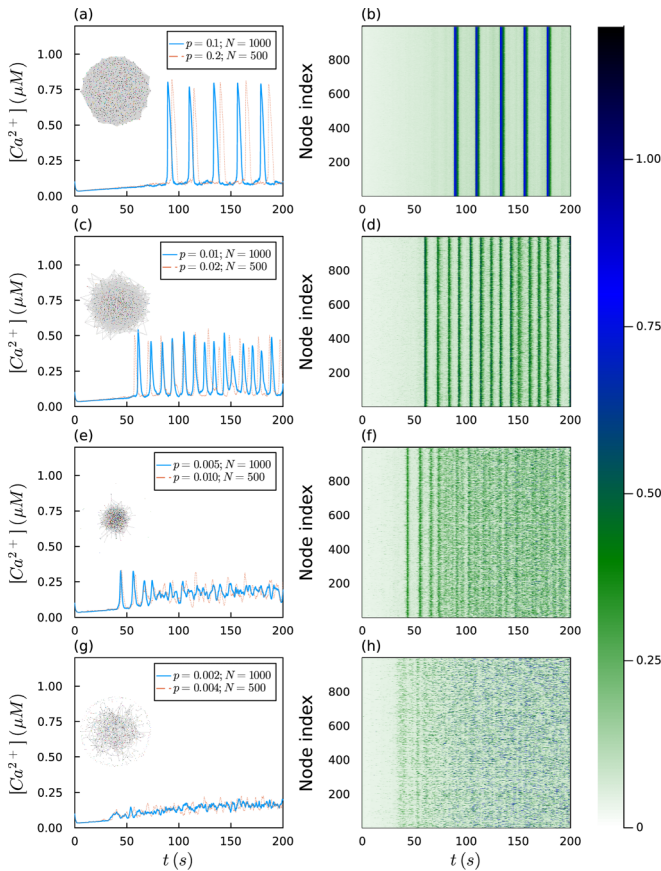


FIG. 3. Evolution of calcium concentration $[Ca^{2+}]$ with the variation of time t on the Erdős-Rényi network. Global calcium concentrations with $p=0.1, 0.01, 0.005, 0.002$ and $N=1000$ (full blue line), with $p=0.2, 0.02, 0.01, 0.004$ and $N=500$ (dashed red line) in (a), (c), (e), (g), respectively. Calcium concentrations for each node with $p=0.1, 0.01, 0.005, 0.002$ and $N = 1000$ are in (b), (d), (f), (h), respectively. The networks with different p and $N = 1000$ are also visualized, and presented in corresponding (a), (c), (e), (g). Other parameters are chosen as those in Fig. 2.

Under such treatment, the size of the network is reduced, but the structure is not changed. The results suggest that the calcium oscillations exhibit almost the same behavior in two cases.

B. BaraBási-Albert network

Different from the Erdős-Rényi network, the BaraBási-Albert network is heterogeneous. The BaraBási-Albert network is generated by adding a sequence of m new nodes to an existing network, so can be denoted as $G_{BA}(N, m)$ [37]. As a scale-free network, hub nodes will emerge and play a more important role in the network dynamics. Recent superresolution nanoscale imaging shows that the cluster sizes satisfy the power law [18,20]. If we take a cluster as a node and assume that the connection ability of a cluster to other clusters is proportional to its size, the network should be a scale-free network. Here we adopt the BaraBási-Albert network to reflect such a characteristic of channel distribution. In Fig. 4, the average amplitude and average interspike interval of calcium oscillations are presented.

In the case of Erdős-Rényi network, the simulation fits the mean-field results very well with large p values. The BaraBási-Albert network exhibits a quite different behavior with large m values where the network is also dense. The maximum can be found at m values of several hundreds, where the large average degrees of the network can also be found. Both amplitude and interspike intervals are close but still below the mean-field results. No stable range such as the Erdős-Rényi network can be found in the case of the BaraBási-Albert network. The interspike interval and amplitude vary with the variation of the m value. If the m value increases further, both amplitude and interspike intervals decrease with the decrease of network density, and deviate further from the mean-field results.

For smaller m , a rapid decrease of the amplitude and interspike interval are found, as in the Erdős-Rényi network. To provide more explicit details, the evolution of the calcium concentration $[Ca^{2+}]$ with the variation of time t on the

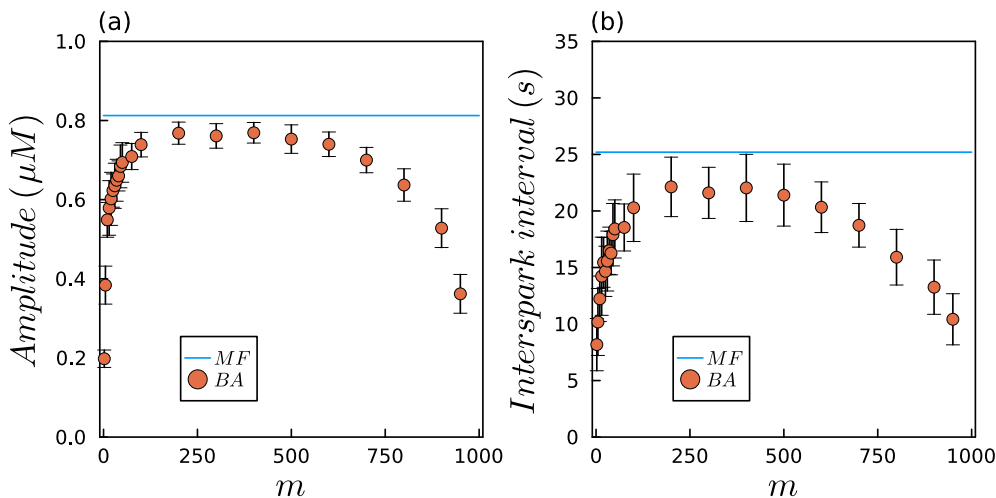


FIG. 4. Average amplitude and interspike interval of calcium oscillations on the BaraBási-Albert (BA) network with the variation of parameters m . The values in mean-field approximation are given as horizontal lines. Other parameters are chosen as those in Fig. 2.

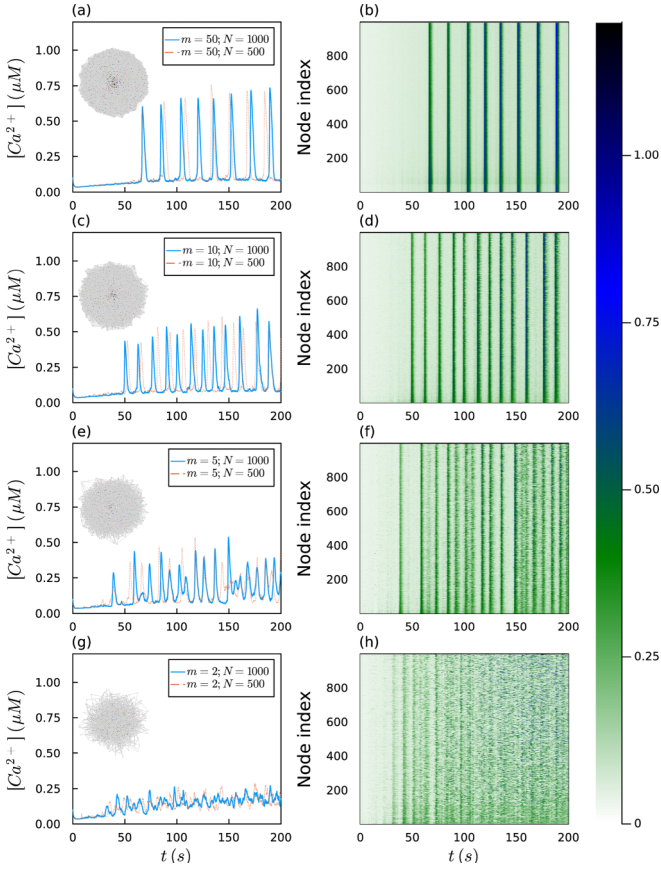


FIG. 5. Evolution of calcium concentration $[Ca^{2+}]$ with the variation of time t on the BaraBási-Albert network. Global calcium concentrations with $m=50, 10, 5, 2$ and $N = 1000$ (full blue line) or $N = 500$ (dashed red line) are in (a), (c), (e), (g), respectively. Calcium concentrations for each node with $m=50, 10, 5, 2$ and $N = 1000$ are in (b), (d), (f), (h), respectively. The networks with different m and $N = 1000$ are also visualized, and presented in (a), (c), (e), (g). Other parameters are chosen as those in Fig. 2.

BaraBási-Albert network is presented in Fig. 5. The calcium concentration $[Ca^{2+}]_i$ for every node is also illustrated.

Since the BaraBási-Albert network with small m value is more important, here, we perform the simulations with $m=50, 10, 5, 2$ and $N=1000$. For network $G_{BA}(1000, 50)$, the average degree is 95, which is almost the same as network $G_{ER}(1000, 0.1)$. The simulation on network $G_{ER}(1000, 0.1)$ is almost the same as the mean-field result, while a large deviation appears in the simulation on network $G_{BA}(1000, 50)$. Obviously, a small amplitude and high frequency can be found, which suggests that the heterogeneous structure seriously affects the calcium oscillation. However, good synchronization is still observed as in network $G_{ER}(1000, 0.1)$, with clear fringes as shown in Fig. 5(b). Most nodes behave in the same manner with the variation of time, which results in a wonderful global oscillation, as shown in Fig. 3(a).

Decreasing the m value will reduce the average degree of the network, which means an increase of global sparsity. With $m=10$ and 5, the oscillation is still reproduced with smaller interspike interval and smaller amplitude, which

deviate further from the results in the mean-field approximation. The desynchronization also appears, which leads to stochastic disturbance on the global oscillation and fluffy on the fringes, as shown in Figs. 3(d) and 3(f). With $m=2$, some nodes are not even connected, the synchronization is almost broken down totally, and the oscillation of global calcium concentration also disappears, as shown in Fig. 5(h).

The network with small size is also introduced to test the effect of node number. The results are presented in Figs. 4(a), 4(c), 4(e), and 4(f) as dashed red lines. Different from the Erdős-Rényi network, the BaraBási-Albert network with the same m value has the same structure except the scale of the network. Here, 500 nodes are considered for checking. The results suggest that the calcium oscillations exhibit almost the same behaviors in two cases.

C. Clique graph

In the literature, many studies were performed locally under the assumption that the cluster is compact and has a regular shape [12,30]. In such a picture, in a cluster, an open channel affects all other channels through calcium releasing. However, the calcium connections between clusters should be weak because the distances between the clusters are assumed to be large. It corresponds to a clique graph, in which several nodes are completely connected, while there is at most one connection between two clusters. The clique graph $G_{cl}(k_c, n)$ consists of n completely connected cliques with k_c nodes. In Fig. 6, we choose four architectures with $N=1000$ nodes and $k_c=100, 20, 10, 5$.

On network $G_{cl}(10, 100)$, 1000 channels are divided into ten clusters with 100 channels. The results suggest that in clusters local oscillation is produced due to local synchronization, as shown in Fig. 6(b). However, weak connections between the clusters make the synchronization between clusters impossible, as shown in Fig. 6(a). Without global synchronization, the local oscillations in clusters cannot merge into a global oscillation. Such results suggest that if the edges of cluster are distinct and the distances between neighbor clusters are too large, the lack of global synchronization will prevent global oscillation.

The current results also contain the information of local dynamics of clusters with different sizes. A large cluster can produce local oscillation with local synchronization. If the size of a cluster is reduced to ten channels, local synchronization is still kept in a cluster. However, the oscillation obviously becomes aperiodic and the interspike interval obviously varies with the time evolution. If cluster size becomes very small, local synchronization is even broken down in a cluster due to the connections with other clusters as shown in Fig. 6(h).

IV. CALCIUM OSCILLATION ON GEOMETRIC NETWORK WITH CLUSTER STRUCTURE

In the previous section, the calcium oscillations on three classic networks are studied. The oscillation can be produced on the homogeneous Erdős-Rényi network with a large enough degree and coincides with the mean-field approximation. On the heterogeneous BaraBási-Albert network, the calcium oscillation can happen, however, it deviates from the

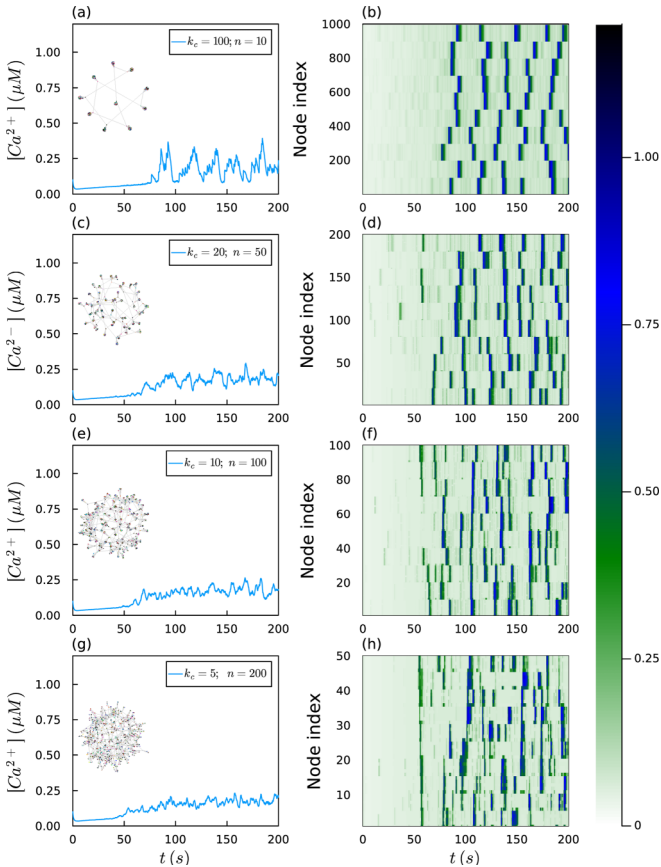


FIG. 6. Evolution of calcium concentration $[Ca^{2+}]$ with the variation of time t on the clique graph network. Global calcium concentrations with $k_c=100, 20, 10, 5$ are in (a), (c), (e), (g), respectively. Calcium concentrations for each node with $k_c=50, 10, 5, 2$ and $N=1000$ are in (b), (d), (f), (h), respectively. The networks with different k_c values are also visualized and presented in (a), (c), (e), (g). Other parameters are chosen as those in Fig. 2.

mean-field approximation with most of the parameter values. The synchronization is found to be important in these two networks. For a sparse network, the oscillation disappears mainly due to the desynchronization. The results on the clique graph network show the importance of the synchronization more clearly. In such a network, the oscillation can be found in every cluster if its size is large enough. However, the connections between the clusters are very weak, which makes the synchronization between the clusters hard to maintain.

The cluster structure has been confirmed by a large amount of experiments. To recover the synchronization, the connections between the clusters should be enhanced, which means that the distances between neighbor clusters should be shortened or more clusters should be added between the existing clusters. However, in the above simulations, the classical networks are introduced directly. The geometric characteristics of the cluster are not included. It makes the understanding of the effect of clusters difficult. In this section, we will introduce a more realistic model to study the calcium oscillation. As said above, the real spatial distribution of calcium channels is very complex. Here, we consider a simple but very

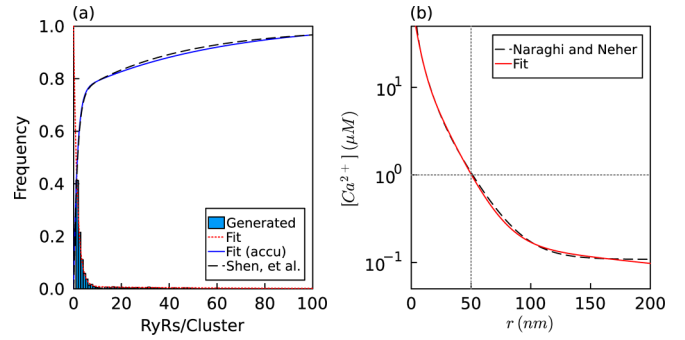


FIG. 7. (a) The frequency distribution of cluster size. The black dashed, blue full, and red dotted lines are for the experimental result by Shen *et al.* [33], fitted accumulated result $g(x)$, and fitted result $f(x)$. The histogram is for the randomly generated result. (b) The calcium gradient against the distance. The black dashed and red full line are for the simulation result in Ref. [39] and fitted result, respectively.

important picture in which all calcium channels distribute on a two-dimensional plane with a cluster structure. In a cell, such spatial distribution can be found in the rough endoplasmic reticulum with a flat-layer shape [52]. In the literature, there exists much information about the cluster structure, which will be adopted to constrain the model to construct a more realistic network for the spatial distribution of calcium channels.

A. Construction of geometric network

The experimental observations suggest that the clusters with random noncompact irregular shapes scatter randomly on the endoplasmic reticulum [18,20,33]. Hence, the spatial distribution of calcium channels should be generated randomly and converted to a network based on experimental information. The geometric network will be constructed in the following steps: (1) randomly generate a series of cluster sizes, (2) randomly generate the clusters with different sizes, (3) randomly distribute the clusters in a two-dimensional plane, and (4) convert the spatial distribution of the RyRs into a geometric network. In the following, the explicit method will be presented.

The most important characteristic of spatial distribution of the calcium channels is the cluster structure. To construct a geometric network reflecting the spatial distribution in a two-dimensional plane, the clusters should be randomly generated first. The observations in Refs. [18,20,33] show that the clusters have different sizes. Hence, the frequency distribution of cluster sizes is required to generate a series of cluster sizes for further generation of clusters. There exist several experimental results about the frequency distribution of cluster sizes in the literature [18,20,33]. Generally speaking, the number of smaller clusters is much larger than these with large size, and the frequency distribution exhibits a power law—that is, the frequency decreases exponentially with the increase of cluster size. In simulations, we adopt the recent experimental data for a two-dimensional surface by Shen *et al.* [33] as a black dashed line in Fig. 7. To randomly generate the cluster sizes, we fit the experimental data with an integral of exponential

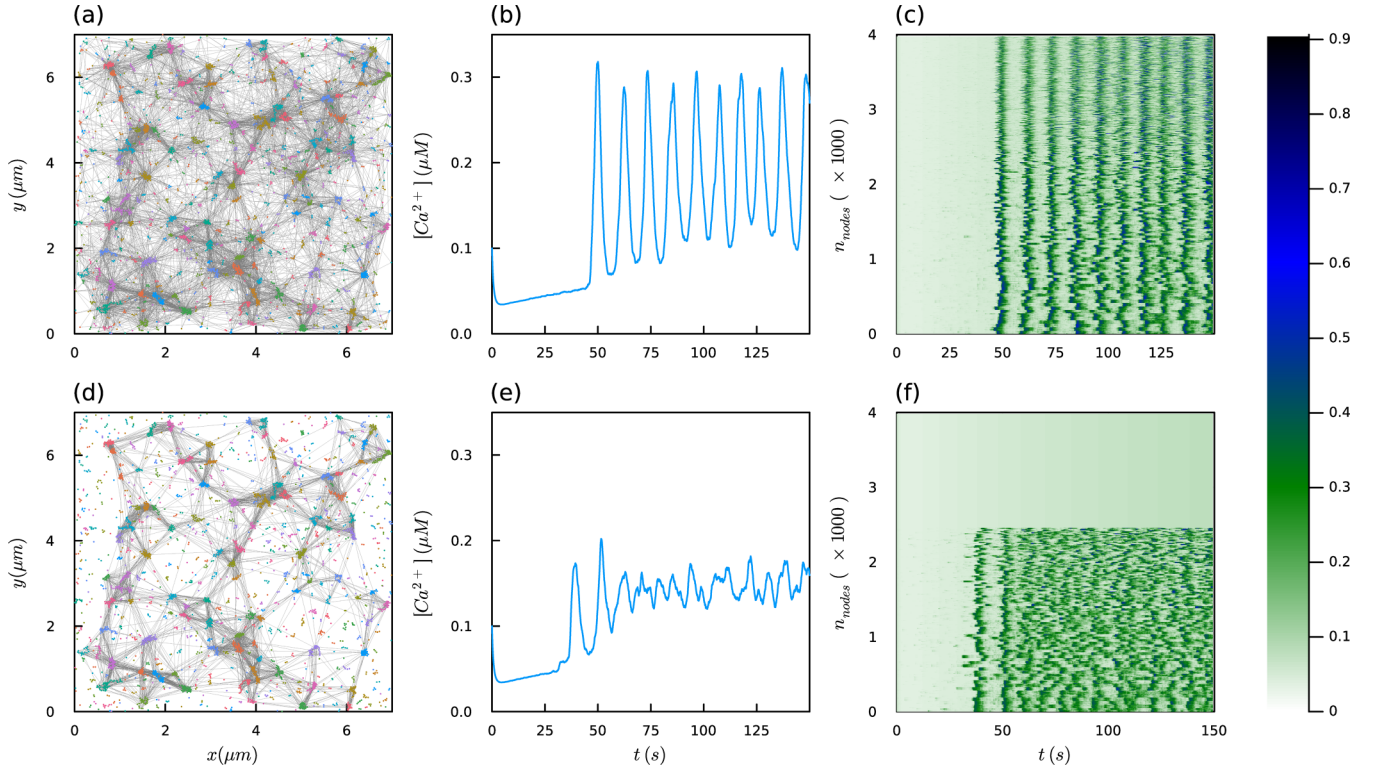


FIG. 8. Calcium oscillation on the geometric network. (a), (d) Spatial distribution of RyRs with random connections. (b), (e) Evolution of the calcium concentration $[Ca^{2+}]$ with variation of time t . (c), (f) Evolution of the calcium concentration $[Ca^{2+}]$ near each RyR with variation of time t . (a)–(c) The network with all clusters considered. (d)–(f) The network without clusters smaller than 10 RyRs.

functions as

$$g(x) = \int_0^x f(y)dy = \int_0^x (ae^{-by} + ce^{-dy})dy. \quad (11)$$

The experimental data of the accumulated frequency distribution are well fitted and shown as the blue solid line in Fig. 7. The normalized function of frequency distribution can be obtained as

$$f(x) = 0.991e^{-0.66x} + 0.009e^{-0.017x}. \quad (12)$$

The first term corresponds to the power law of the frequency distribution. The second term is for an enhancement of small size clusters, which has been observed in many experiments [18,33].

With the obtained frequency distribution, a series of cluster sizes can be generated. In the current paper, we consider $N = 4000$ channels. Two random numbers are introduced as r_1 in $[0,1]$ and r_2 in $[0, n_{\max}]$. Here, we only consider the cluster sizes which are not too large to avoid the uncertainty introduced by extremely large cluster in a limited area considered. A maximum size of the cluster as $n_{\max} = 100$ is adopted in simulations. It is also consistent with the experimental observation, in which the clusters composed of more than 100 RyRs were scarcely observed [18,20,33]. If $r_1 < f(r_2)$, the r_2 will be recorded as a value of cluster size. If not, these two random numbers are discarded. Then, another two random numbers are generated and judgement is repeated until the total number of RyRs reaches the total number of channels N . The frequency distribution of generated 783 cluster sizes is also presented and compared with the fitted function $f(x)$

in Fig. 7 (we would like to note that all clusters with size 0 are discarded). One can find that the experimental frequency distribution is well generated with the above method.

In the above step, a series of cluster sizes are randomly generated. In the following, clusters with these sizes will be generated. In the literature, the structure of a cluster is found to be complex. In this paper, we adopt the picture suggested by the superresolution imaging in Ref. [20]. The observations suggest that the cluster is not compact and the shape is irregular. Fortunately, in that paper, the authors also provided a method to randomly generate a cluster, which is adopted directly in the current paper. The simulation starts with an original position $\mathbf{x}_1 = (0, 0)$, which is recorded in a vector as the position of the first RyR. Then, a random direction θ is generated with a distance r which is varied slightly around a mean distance of 40 nm according to a Gaussian distribution with a sigma of 7.4 nm. It closely matches the observed distance distribution in mean and width in Ref. [20]. The position moves to $\mathbf{x}_2 = \mathbf{x}_1 + \Delta\mathbf{x}$ with a translation $\Delta\mathbf{x} = (r \cos \theta, r \sin \theta)$. The position \mathbf{x}_2 is recorded in the vector as position of the second RyR. Then, another random direction and distance are generated. The new translation is added into previous position \mathbf{x}_2 , and a new position \mathbf{x}_3 is obtained and recorded again. The steps continue until the RyR position series of a cluster with certain size is obtained and recorded in the vector. As shown in Fig. 8(a), this self-assembly process leads to the appearance of some larger gaps in the clusters similar to those observed in Ref. [20].

The randomly generated clusters with different sizes need to be scattered randomly in a two-dimensional plane. In the

literature [34], the role of the Rogue and clustered RyRs in a two-dimensional plane was also discussed, and the rogue RyRs were found important in the generation of calcium sparks. In that work, the clustered and Rogue RyRs were grouped into a CRU (Ca^{2+} release units). However, in many observations [18,20,33], the clusters with different sizes distribute randomly, which is adopted in the current paper. A square region with a length of $l = d\sqrt{N_{\text{cluster}}}$ is considered with d and N_{cluster} being the mean distance between two neighbor clusters and total number of clusters. The distribution of nearest-neighbor distances was studied in the literature, and the largest possibility appears at about 200 nm with a long tail [20]. In the current paper, we adopt a mean distance as 250 nm. For a cluster, two random numbers in range $[0, l]$ are generated as the position of the cluster, which is added into the positions of all RyRs in the cluster obtained in the previous step. If the clusters are spread randomly in the two-dimensional plane directly, some clusters may overlap to each other. To avoid such overlapping, we divide the two-dimensional square region into lattices of $30 \times 30 \text{ nm}^2$. When the positions of the RyRs in a cluster are determined, the occupied lattices are marked and cannot be occupied again. With such treatment, a random spread of the clusters is reached, and shown in Fig. 8(a).

In our theoretical frame, the connections should be described by an adjacency matrix. Hence, the last step to construct the geometric network is to abstract the RyR distribution in a two-dimensional plane into nodes and edges of a network. Obviously, the RyRs should be taken as nodes of the geometric network. In Sec. III, the edges are introduced according to the classical networks where only the characteristics of the RyR distribution are considered. In the current case, an explicit transition from the distance between a RyR pair to a edge of network is required. The connection should reflect the magnitude of variation of calcium concentration. As discussed in Sec. II, the buildup of calcium gradient between two RyRs is much faster than the activation of RyRs [27,41,42]. Hence, the connection of two RyRs can be determined by the calcium gradient arising from the open channel. The estimation of the calcium gradient is beyond the scope of this paper. We adopt the simulation results in Ref. [39] as shown in Fig. 7. It suggests a rapid decrease of the calcium concentration with the distance between two channels, which becomes slower at distance larger than about 100 nm. To make the further transition, it is fitted in a range from 2 nm to 200 nm by three exponential functions as

$$c(r) = 77.7e^{-r/4.3} + 21.7e^{-r/15.5} + 0.19e^{-r/300}, \quad (13)$$

where the r is the distance between two channels. Here, we neglect very small distances where the calcium concentration is very large. In fact, we connect all channel pairs with a distance smaller than 50 nm, corresponding to $1 \mu\text{M}$, which is smaller than the size of two channels. For other channel pairs, the probability to have a connection is determined by the calcium concentration with the following method. A random number is generated and compared with $c(r)$, with r being the distance of two channels. If the random number is smaller, the two channels will be connected. The results are also presented in Fig. 8(a).

B. Simulation of oscillations on geometric network

With the method in the above, a spatial distribution of 4000 RyRs in a two-dimensional square region of $7 \times 7 \mu\text{m}^2$ is generated, as shown in Fig. 8(a). The RyRs are grouped into 783 clusters with different sizes, which are noncompact, and have irregular shapes as in experimental observations. A large amount of small clusters and rogue RyRs scatter around the large clusters. The connections of the RyRs in the large clusters are dense. However, different from the clique graph, the RyRs in a large cluster are not fully connected due to the irregular shape.

The network in Fig. 8(a) can be described with an adjacency matrix A in Eq. (2). The average degree of the obtained network is about 10. Considering the total number of RyRs of 4000, the geometric network is a sparse network. Such a network has a sparsity close to those of a Erdős-Rényi network $G_{\text{ER}}(1000, 0.002)$ in Fig. 3(g) and a Barabási-Albert network $G_{\text{ER}}(1000, 2)$ in Fig. 5(g), which cannot produce a calcium oscillation. With the adjacency matrix, the evolution of the calcium concentration can be simulated with the same procedure as for the classical networks. With the same parameters of the calcium transduction mechanism, one can find that the calcium oscillation can be reproduced, as shown in Fig. 8(b). The evolution of calcium concentrations near 4000 RyRs are presented in Fig. 8(c). The results suggest that the synchronization can be kept well. These results suggest that the geometric network based on the experimental information has better performance than the Erdős-Rényi or Barabási-Albert network with the same sparsity.

To understand the role of small clusters and rogue RyRs, the connections to RyRs in all clusters with sizes smaller than 10 RyRs are removed, as shown in Fig. 8(d). For comparison with the results with all clusters, the small clusters and rogue RyRs are kept in the figure. One can find that the sketch of the connections between clusters is still kept. Although the large clusters are still connected, as shown in Fig. 8(e), the calcium oscillation disappears after removing the small clusters. In Fig. 8(f), the time revolution of every RyR is illustrated. No oscillation happens near the rogue RyRs and small clusters whose connections are removed. The oscillation still can be seen for a single large cluster, though not so well. However, the global calcium oscillation fails, as on the clique graph network, due to the desynchronization of different clusters. The synchronization cannot be maintained only with connections between the large clusters. The results support the importance of the small clusters and rogue RyRs in the formation and maintenance of calcium oscillation.

V. SUMMARY AND DISCUSSION

The calcium oscillation is a physiological phenomenon, which is very important to regulate intracellular life activity, and abnormal amplitude and frequency have a close relationship to many diseases. The calcium channel is a key ingredient in the calcium regulation mechanism to reproduce the calcium oscillation. Though there exist many models which are successful to reproduce the oscillations, the effect of the spatial distribution of calcium channels beyond the cluster is scarcely investigated in existing studies. In this paper, we

establish a theoretical framework beyond the existing models to study the effect of the spatial distribution on the calcium oscillation. The Keizer-Levine model is introduced to describe the transition of four states of the calcium channel, and calcium exchange between the cytoplasm and the stores or external medium. Since the Keizer-Levine model is enough to successfully generate the calcium oscillation, in the current paper the mechanism is extended directly from the Keizer-Levine model under the mean-field ansatz to a network model. The variation of the calcium concentration induced by the open channels is described by an adjacency matrix of considered networks with channels as nodes and Ca^{2+} connections as edges. The theoretical frame is checked first by the complete graph, and the mean-field result is well reproduced.

Since the real spatial distribution of the calcium channels is very complex, several types of classical networks, which reflect different sides of characteristics of channel distribution, are introduced to perform simulation. The Erdős-Rényi network reflects the homogeneous distribution at large scale. The heterogeneous Barabási-Albert network reflects a power law of cluster sizes, in which clusters are taken as nodes. For the Erdős-Rényi network, if parameter p is chosen larger than 0.1, the interspike interval and amplitude are almost the same as the results in the mean-field approximation with some uncertainties from the randomness introduced in the simulation. Different from the Erdős-Rényi network, the Barabási-Albert network deviates from the mean-field approximation in almost a full range of the parameters. If the parameters are justified, the Barabási-Albert network can produce an oscillation with a similar frequency and amplitude as the Erdős-Rényi network. It may be the reason why the models under mean-field ansatz are also successful to describe many experimental observations. However, the Erdős-Rényi network lacks the regulation ability of the Barabási-Albert network by changing the architectures. The modulation of frequency and the amplitude of calcium oscillation is important to intracellular life activity [54], such as sensitive and specific response of the effector proteins [55]. For both the Erdős-Rényi and Barabási-Albert networks which are not very sparse, the synchronization of the nodes is very well, which makes global oscillation possible. If the network becomes sparse, which means that the couplings between nodes are far from a global coupling, the synchronization is broken down with the increase of the sparsity, as suggested in Ref. [56]. With the increase of sparsity of network, the frequency increases and the amplitude decreases. For a very sparse network, the synchronization, as well as oscillation, will disappear.

In the clique graph and geometric network, the cluster structure is considered explicitly. Cluster structure is a well-known and important characteristic of channel distribution. Early observations suggest that RyRs in a cluster are packed compactly, forming a tight lattice [17]. Such a picture was also adopted in many studies focusing on the local dynamics [12,21,30]. To reflect such a characteristic, a simulation is performed with a clique graph in which the channels in a cluster are fully connected. The results suggest that local oscillation and local synchronization can be reproduced in the cluster if its size is large enough. The global oscillation does not exist

due to the desynchronization between clusters. It suggests that a regular compact picture of clusters with a relatively large distance between the clusters is not suitable to describe the realistic channel distribution. Besides the clique graph, a geometric network is constructed in a two-dimensional plane with the experimental information in Refs. [18,20,25]. The cluster sizes are randomly generated with the experimental frequency distribution. The RyR arrangements of a series of clusters with different sizes are simulated randomly with the experimental mean distance. The calcium oscillation can be well reproduced from the geometric network with the cluster structure. As shown in Fig. 8(f), about two-thirds of the RyRs distribute in clusters larger than 10 RyRs. However, if the RyRs in small clusters are removed, the synchronization between the clusters cannot be maintained, though the sketch of the connections is still kept. Such results suggest the importance of small clusters in the formation and maintenance of calcium oscillation.

In summary, a theoretical framework is first established to study the spatial distribution of calcium channels with complex structures by simulating the calcium oscillation on three classical networks and a more realistic geometric network. The mean-field result can be well reproduced in the simulations on the homogeneous networks. The power law of cluster sizes is referred to due to more effectivity to modulate calcium oscillation. The simple cluster model is disfavored due to the desynchronization between the clusters. However, with the small clusters included, the calcium oscillation can be reproduced. The recent superresolution nanoscale imaging supports such conclusion [18,20,25].

The current research provides a helpful basis to construct a more realistic model to study the channel distribution, and can be extended to study other phenomena in calcium signal transduction. However, in the current paper, the diffusion of calcium is only included as the connection between calcium channels while the delay time is neglected. The diffusion of the free calcium should be compared with the open time of the RyR. Hence, the time delay between the RyRs can safely be neglected for free calcium. The buffers, such as calmodulin, will make calcium diffuse slower than free calcium. Considering that the buffers will carry calcium far from the endoplasmic reticulum, in the current model we assume that the calcium once attached to buffers does not affect the calcium channels. In fact, its effect can be partly absorbed into the influx and efflux, which exchange calcium with an external medium. In the current paper, the effect of the diffusion is not fully included. The effectiveness of such treatment needs further studies, such as simulation of the calcium spark. In addition, the current paper is based on the Keizer-Levine model, in which some ingredients are not included, such as the variation and diffusion of the calcium in endoplasmic reticulum. Also, the mechanism about buffers is also not introduced explicitly. To extend the current framework to study more experimental phenomena, a more suitable mechanism should be included to establish the network model.

ACKNOWLEDGMENT

This project is supported by the National Natural Science Foundation of China (Grant No. 11675228).

- [1] M. J. Berridge, The inositol trisphosphate/calcium signaling pathway in health and disease, *Physiol. Rev.* **96**, 1261 (2016).
- [2] D. Terentyev, I. Györke, A. E. Belevych, R. Terentyeva, A. Sridhar, Y. Nishijima, E. C. de Blanco, S. Khanna, C. K. Sen, A. J. Cardounel *et al.*, Redox modification of ryanodine receptors contributes to sarcoplasmic reticulum Ca^{2+} leak in chronic heart failure, *Circ. Res.* **103**, 1466 (2008).
- [3] B. Fiedler, S. M. Lohmann, A. Smolenski, S. Linnemüller, B. Pieske, F. Schröder, J. D. Molkenkin, H. Drexler, and K. C. Wollert, Inhibition of calcineurin-NFAT hypertrophy signaling by cGMP-dependent protein kinase type I in cardiac myocytes, *Proc. Natl. Acad. Sci. USA* **99**, 11363 (2002).
- [4] O. Cohen and S. A. Safran, Physics of spontaneous calcium oscillations in cardiac cells and their entrainment, *Phys. Rev. Lett.* **122**, 198101 (2019).
- [5] J. Wei, J. Yao, D. Belke, W. Guo, X. Zhong, B. Sun, R. Wang, J. P. Estillore, A. Vallmitjana, R. Benitez *et al.*, Ca^{2+} -CaM dependent inactivation of RyR2 underlies Ca^{2+} alternans in intact heart, *Circ. Res.* **128**, e63-e83 (2021).
- [6] J. Sneyd, J. M. Han, L. Wang, J. Chen, X. Yang, A. Tanimura, M. J. Sanderson, V. Kirk, and D. I. Yule, On the dynamical structure of calcium oscillations, *Proc. Natl. Acad. Sci. USA* **114**, 1456 (2017).
- [7] E. Smedler and P. Uhlén, Frequency decoding of calcium oscillations, *Biochim. Biophys. Acta, Gen. Subj.* **1840**, 964 (2014).
- [8] G. W. De Yong and J. Keizer, A single-pool inositol 1, 4, 5-trisphosphate-receptor-based model for agonist-stimulated oscillations in Ca^{2+} concentration, *Proc. Natl. Acad. Sci. USA* **89**, 9895 (1992).
- [9] J. Keizer and L. Levine, Ryanodine receptor adaptation and Ca^{2+} -induced Ca^{2+} release-dependent Ca^{2+} oscillations, *Biophys. J.* **71**, 3477 (1996).
- [10] J. Sneyd and J. F. Dufour, A dynamic model of the type-2 inositol trisphosphate receptor, *Proc. Natl. Acad. Sci. USA* **99**, 2398 (2002).
- [11] H. Cheng and W. J. Lederer, Calcium sparks, *Physiol. Rev.* **88**, 1491 (2008).
- [12] S. Rüdiger, J. W. Shuai, and I. M. Sokolov, Law of Mass Action, Detailed Balance, and the Modeling of Calcium Puffs, *Phys. Rev. Lett.* **105**, 048103 (2010).
- [13] S. Rüdiger, P. Jung, and J. W. Shuai, Termination of Ca^{2+} release for clustered IP3R channels, *PLoS Comput. Biol.* **8**, e1002485 (2012).
- [14] C. P. Fall and J. E. Keizer, Mitochondrial modulation of intracellular Ca^{2+} signaling, *J. Theor. Biol.* **210**, 151 (2001).
- [15] M. Marhl, T. Haberichter, M. Brumen, and R. Heinrich, Complex calcium oscillations and the role of mitochondria and cytosolic proteins, *Biosystems* **57**, 75 (2000).
- [16] P. Szopa, M. Dyzma, B. Kźmierczak, Membrane associated complexes in calcium dynamics modelling, *Phys. Biol.* **10**, 035004 (2013).
- [17] C. Franzini-Armstrong, F. Protasi, V. Ramesh, Shape, size, and distribution of Ca^{2+} release units and couplons in skeletal and cardiac muscles, *Biophys. J.* **77**, 1528 (1999).
- [18] D. Baddeley, I. D. Jayasinghe, L. Lam, S. Rossberger, M. B. Cannell, and C. Soeller, Optical single-channel resolution imaging of the ryanodine receptor distribution in rat cardiac myocytes, *Proc. Natl. Acad. Sci. USA* **106**, 22275 (2009).
- [19] I. F. Smith and I. Parker, Imaging the quantal substructure of single IP₃R channel activity during Ca^{2+} puffs in intact mammalian cells, *Proc. Natl. Acad. Sci. USA* **106**, 6404 (2009).
- [20] I. Jayasinghe, A. H. Clowsley, R. Lin, T. Lutz, C. Harrison, E. Green, D. Baddeley, L. D. Michele, and C. Soeller, True molecular scale visualization of variable clustering properties of ryanodine receptors, *Cell Rep.* **22**, 557 (2018).
- [21] P. Cao, G. Donovan, M. Falcke, and J. Sneyd, A stochastic model of calcium puffs based on single-channel data, *Biophys. J.* **105**, 1133 (2013).
- [22] M. A. Walker, G. S. B. Williams, T. Kohl, S. E. Lehnart, M. S. Jafri, J. L. Greenstein, W. J. Lederer and R. L. Winslow, Super-resolution modeling of calcium release in the heart, *Biophys. J.* **107**, 3018 (2014).
- [23] M. A. Walker, T. Kohl, S. E. Lehnart, J. L. Greenstein, W. J. Lederer, and R. L. Winslow, On the adjacency matrix of RyR2 cluster structures, *PLoS Comput. Biol.* **11**, e1004521 (2015).
- [24] M. H. Mesa, J. van den Brink, and W. E. Louch, Nanoscale organization of ryanodine receptor distribution and phosphorylation pattern determines the dynamics of calcium sparks, *PLOS Comput. Biol.* **18**, e1010126 (2021).
- [25] S. A. Tiscione, M. Casas, J. D. Horvath, V. Lam, K. Hino, D. S. Ory, L. F. Santana, S. Simó, R. E. Dixon and E. J. Dickson, IP₃R-driven increases in mitochondrial Ca^{2+} promote neuronal death in NPC disease, *Proc. Natl. Acad. Sci. USA* **118**, e2110629118 (2021).
- [26] B. I. Iaparov, A. S. Moskvina, I. Zahradník, and A. Zahradníková, Stochastic and deterministic approaches to modelling calcium release in cardiac myocytes at different spatial arrangements of ryanodine receptors, *Eur. Biophys. J.* **48**, 579 (2019).
- [27] B. I. Iaparov, I. Zahradník, A. S. Moskvina, and A. Zahradníková, In silico simulations reveal that RYR distribution affects the dynamics of calcium release in cardiac myocytes, *J. Gen. Physiol.* **153**, e202012685 (2021).
- [28] M. B. Cannell, C. H. T. Kong, M. S. Imtiaz, and D. R. Laver, Control of sarcoplasmic reticulum Ca^{2+} release by stochastic RyR gating within a 3D model of the cardiac dyad and importance of induction decay for CICR termination, *Biophys. J.* **104**, 2149 (2013).
- [29] A. J. Tanskanen, J. L. Greenstein, A. Chen, S. X. Sun, and R. L. Winslow, Protein geometry and placement in the cardiac dyad influence macroscopic properties of calcium-induced calcium release, *Biophys. J.* **92**, 3379 (2007).
- [30] H. Qi, Y. Huang, S. Rüdiger, and J. Shuai, Frequency and relative prevalence of calcium blips and puffs in a model of small IP3R clusters, *Biophys. J.* **106**, 2353 (2014).
- [31] Y. Xie, Y. Yang, S. Galice, D. M. Bers, and D. Sato, Size matters: Ryanodine receptor cluster size heterogeneity potentiates calcium waves, *Biophys. J.* **116**, 530 (2019).
- [32] S. Galice, Y. Xie, Y. Yang, D. Sato, and D. M. Bers, Size matters: Ryanodine receptor cluster size affects arrhythmogenic sarcoplasmic reticulum calcium release, *J. Am. Heart Assoc.* **7**, e008724 (2018).
- [33] X. Shen, J. van den Brink, Y. Hou, D. Colli, C. Le, T. R. Kolstad, N. MacQuaide, C. R. Carlson, P. M. Kekenus-Huskey, A. G. Edwards *et al.*, 3D dSTORM imaging reveals novel detail of ryanodine receptor localization in rat cardiac myocytes, *J. Physiol.* **597**, 399 (2019).

- [34] X. Chen, Y. Feng, Y. Huo, and W. Tan, The interplay of rogue and clustered ryanodine receptors regulates Ca^{2+} waves in cardiac myocytes, *Front. Physiol.* **9**, 393 (2018).
- [35] G. Hernandez-Hernandez, J. Myers, E. Alvarez-Lacalle, and Y. Shiferaw, Nonlinear signaling on biological networks: The role of stochasticity and spectral clustering, *Phys. Rev. E* **95**, 032313 (2017).
- [36] H.-Y. Jiang and J. He, Nonlinear signal transduction network with multistate, *Chin. Phys. B* **30**, 118703 (2021).
- [37] A. L. Barabási and R. Albert, Emergence of Scaling in Random Networks, *Science* **286**, 509 (1999).
- [38] H. Y. Jiang and J. He, Three-dimensional cytoplasmic calcium propagation with boundaries, *Commun. Theor. Phys.* **73**, 015601 (2021).
- [39] M. Naraghi and E. Neher, Linearized buffered Ca^{2+} diffusion in microdomains and its implications for calculation of $[\text{Ca}^{2+}]$ at the mouth of a calcium channel, *J. Neurosci.* **17**, 6961 (1997).
- [40] A. Zahradníková, M. Dura, I. Györke, A. L. Escobar, I. Zahradník, and S. Györke, Regulation of dynamic behavior of cardiac ryanodine receptor by Mg^{2+} under simulated physiological conditions, *Am. J. Physiol. Cell Physiol.* **285**, C1059 (2003).
- [41] C. Soeller and M. B. Cannell, Numerical simulation of local calcium movements during L-type calcium channel gating in the cardiac diad, *Biophys. J.* **73**, 97 (1997).
- [42] I. Valent, A. Zahradníková, J. Pavelková, and I. Zahradník, Spatial and temporal Ca^{2+} , Mg^{2+} , and ATP2-dynamics in cardiac dyads during calcium release, *Biochim. Biophys. Acta, Rev. Biomembr.* **1768**, 155 (2007).
- [43] S. Györke and M. Fill, Ryanodine receptor adaptation: Control mechanism of Ca^{2+} -induced Ca^{2+} release in heart, *Science* **260**, 807 (1993).
- [44] A. Tse, F. W. Tse, and B. Hille, Calcium homeostasis in identified rat gonadotrophs, *J. Physiol.* **477**, 511 (1994).
- [45] D. D. Friel, $[\text{Ca}^{2+}]_i$ oscillations in sympathetic neurons: an experimental test of a theoretical model, *Biophys. J.* **68**, 1752 (1995).
- [46] B. Alberts, D. Bray, J. Lewis, M. Raff, K. Roberts, and J. D. Watson, *Molecular Biology of the Cell*, 2nd ed. (Garland, New York, 1998).
- [47] E. Carafoli, Biogenesis: Plasma membrane calcium ATPase: 15 years of work on the purified enzyme, *FASEB J.* **8**, 993 (1994).
- [48] A. V. Tepikin, S. G. Voronina, D. V. Gallacher, and O. H. Petersen, Pulsatile Ca^{2+} extrusion from single pancreatic acinar cells during receptor-activated cytosolic Ca^{2+} spiking, *J. Biol. Chem.* **267**, 14073 (1992).
- [49] J. Lytton, M. Westlin, S. E. Burk, G. E. Shull, and D. H. MacLennan, Functional comparisons between isoforms of the sarcoplasmic or endoplasmic reticulum family of calcium pumps, *J. Biol. Chem.* **267**, 14483 (1992).
- [50] D. T. Gillespie, Exact stochastic simulation of coupled chemical reactions, *J. Phys. Chem.* **81**, 2340 (1977).
- [51] J. Rothman, Mechanisms of intracellular protein transport, *Nature (London)* **372**, 55 (1994).
- [52] Y. Shibata, G. K. Voeltz, and T. A. Rapoport, Rough sheets and smooth tubules, *Cell* **126**, 435 (2006).
- [53] M. E. J. Newman, *Networks: An Introduction* (Oxford University Press, Oxford, New York, 2010).
- [54] S. J. P. Pratt, E. Hernández-Ochoa, and S. S. Martin, Calcium signaling: Breast cancer's approach to manipulation of cellular circuitry, *Biophys. Rev.* **12**, 1343 (2020).
- [55] R. E. Dolmetsch, K. Xu, and R. S. Lewis, Calcium oscillations increase the efficiency and specificity of gene expression, *Nature (London)* **392**, 933 (1998).
- [56] E. Baspinar, L. Schülen, S. Olmi, and A. Zakharova, Coherence resonance in neuronal populations: Mean-field versus network model, *Phys. Rev. E* **103**, 032308 (2021).